Volum 36, Nos. 1–3
May 1991
Edit r: Eln

ENG

F

ultramicroscopy

An International Journal affiliated with EMSA, ISEM, SCANDEM, NVEM, SGOEM, SIME-SM, DGE, MSC and ASEM

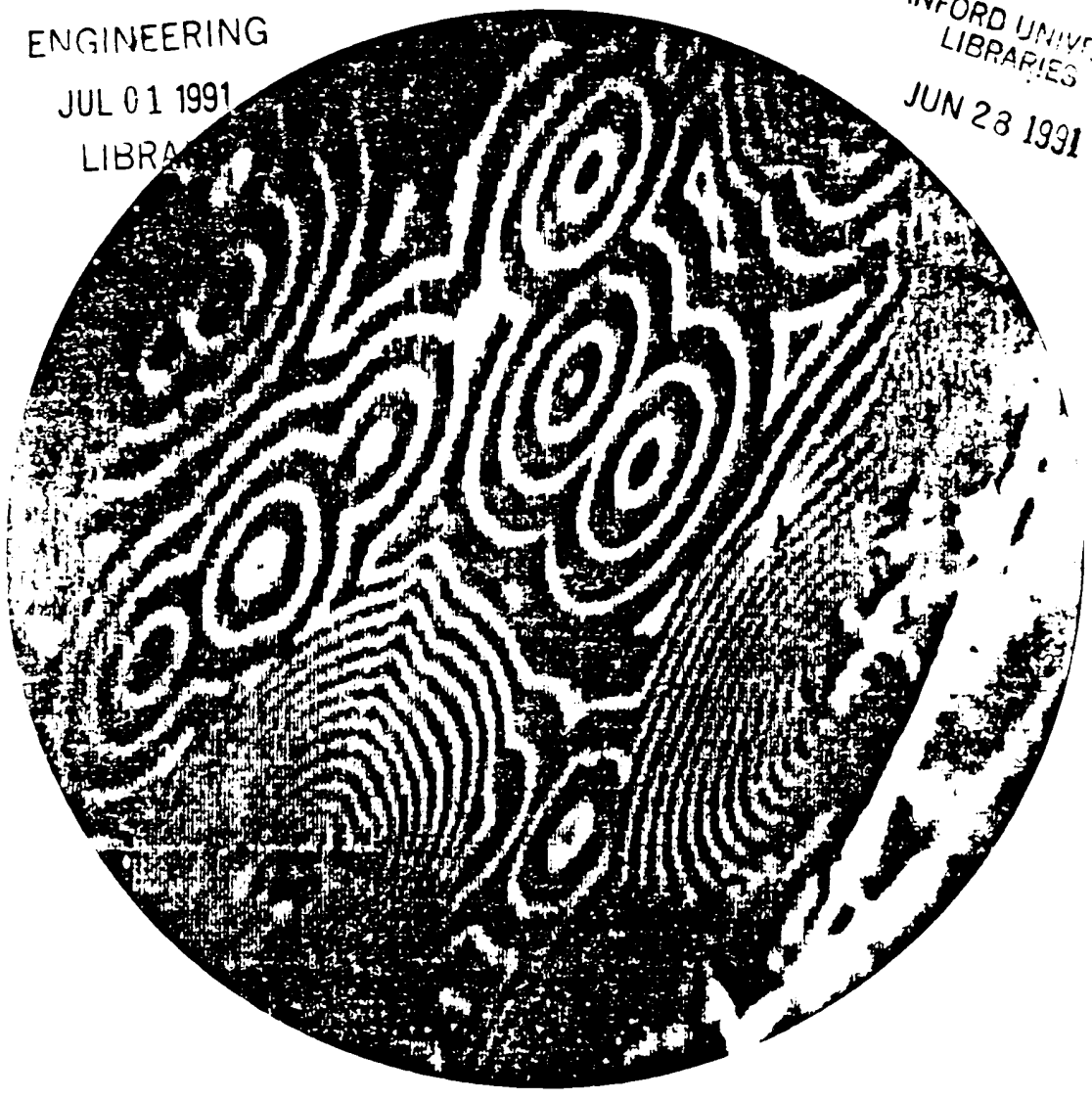

This issue is part of the 1990 subscription program
To be followed by Volume 35, Number 3

NORTH-HOLLAND

ULTRDG 36(1–3) 1–274 (1991)

Ultramicroscopy 36 (1991) 76–90
North-Holland

Design of a spectroscopic low-energy electron microscope

Lee H. Veneklasen [1]
Physikalisches Institut der TU Clausthal, W-3392 Clausthal-Zellerfeld, Germany

Received 17 August 1990; at Editorial Office 1 December 1990

The instrumental design aspects of a spectroscopic low-energy electron microscope for the direct imaging of chemical, topographic and structural features on surfaces are presented. This instrument extends the LEEM concept to include energy-resolved imaging of secondary, Auger and X-ray emissions with enhanced resolution and collection efficiency. Key new elements include a triode magnetic cathode lens, a prism array separator magnet, a decelerating hemispherical energy analyzer, and a high-quantum-efficiency intensifier. Mathematical techniques for the optimization of viewing conditions are reviewed, and the goals of pending performance tests are given.

1. Introduction

The low-energy electron microscope (LEEM) is not a common instrument, but its evolution spans the history of electron microscopy. From the viewpoint of electron-optical configuration, it contains two key elements: the cathode immersion lens and the beam separator. The cathode lens was first applied in photoemission microscopy (PEEM) [1]. The same lens can be used with a bidirectional beam for mirror microscopy, or as a cathode lens diffractometer for low-energy electron diffraction (MEMLEED) [21]. With the addition of a magnetic prism beam separator that allows separate manipulation of the illumination and imaging beam, the optical system becomes the surface-imaging equivalent of a transmission microscope objective lens, and most familiar TEM contrast modes may be exploited. In particular, low-energy backscattered electrons have been used to study the dynamics of atomic step structure, phase transitions, and epitaxial growth upon crystalline surfaces using phase and diffraction contrast [3–5]. In this paper, the term LEEM will be used to cover all direct imaging and diffraction modes using a cathode–lens beam-separator system.

The instrument described here is the next logical step in the development – that is, to try to obtain images using characteristic secondary emission electrons [5]. The addition of an imaging energy analyser should not only allow chemical contrast, but should also dramatically improve the resolution of secondary and elastic backscatter images. The ultimate instrumental goal is favorable spatial *and* temporal resolution in chemical, topographic and structure-sensitive imaging modes, in the hope that this complementary information will lead to a more complete understanding of surface processes.

A direct-imaging instrument seems to offer fundamental advantages, especially for fast chemical mapping. Many individual image elements may be illuminated and recorded in parallel. If the imaging optics can collect a favorable fraction of the characteristic emissions, it is easier to combine high spatial resolution with short integration times. Performance predictions are not straightforward, and may be limited by unexpected effects, but it seems that the imaging system will offer new opportunities. A model computation, that includes optimization techniques for scanning and direct-imaging instruments, is offered in the accompany-

[1] Present address: KLA Instruments Inc., 3520 Bassett Street, Santa Clara, CA 95052, USA.

0304-3991/91/$03.50

ing paper [6]. The goal of this paper is to review a specific design in more detail.

The original LEEM instrument of Bauer and Telieps has been redesigned and built in a more compact, user-friendly configuration. This "LEEM II" instrument, shown in fig. 1, has been in operation for about one year. Key improvements include a more flexible LaB_6 gun and triple condenser lens system, a wider magnification range, selected-area and low-angle diffraction modes, and a UHV airlock system. It has proven to be comparable to the original instrument in resolution and image quality, and better in LEED performance, environmental insensitivity, specimen manipulation and environmental control.

The spectroscopic LEEM described in this paper is a rebuild of the LEEM II instrument [7]. New changes include the addition of a magnetic triode objective lens, an imaging energy analyzer, a revised specimen and gun-biasing system, and an improved image intensifier.

There are two basic setups, for elastic and inelastic secondary imaging. The elastic mode uses mirrored or backscattered electrons that are scattered coherently without energy loss. Incident and reflected energy is determined by the potential difference between the electron source and sample. Since the sample is in an electric field, mirror mode is particularly sensitive to both submicron-scale topography and surface potential. Elastic backscattering at low voltages has a high yield and low penetration, and is particularly sensitive to atomic-scale lattice and step structure. Using parallel, coherent illumination, crystalline

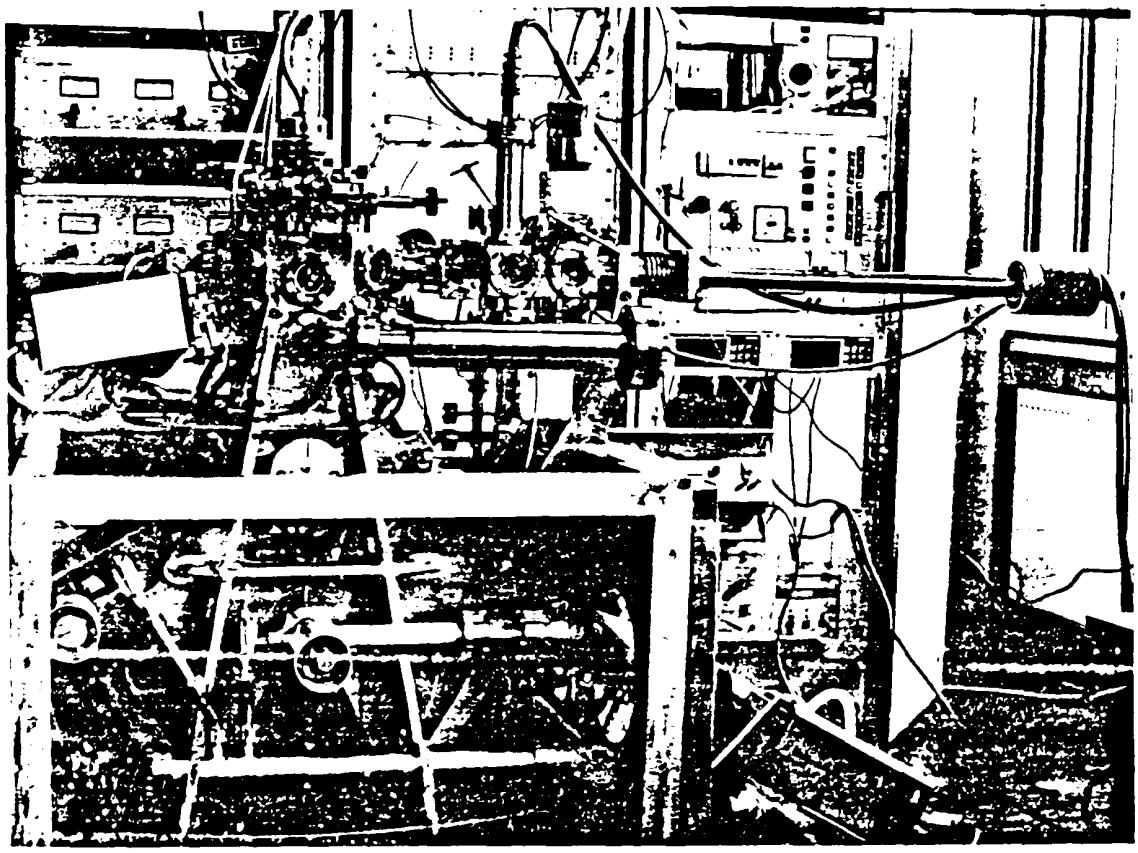

Fig. 1. Photograph of the LEEM II instrument from which the SPEC LEEM will be constructed.

samples show a well defined LEED diffraction pattern at the objective lens back focal plane. The collimating action of the accelerating field, whose strength depends upon the square root of the initial energy, exactly cancels the energy dependence of the diffraction angle; thus the size of the diffraction pattern is independent of initial starting voltage. Using an objective aperture to mask all but the zero-order reflexes, diffraction contrast depends upon diffracted intensity. By appropriate choice of start voltage, regions of differing surface structure become visible.

At low voltage, the electron wavelength is comparable to monatomic step heights. This gives rise to interference and near-field Fresnel diffraction, or phase contrast. With slight defocus, atomic steps can be imaged, and their motion and influence upon phase transitions, domain boundaries, and epitaxial growth may be studied [4]. The instrument also allows photo- and thermionic-emission imaging.

Imaging with higher-energy secondary emissions has not yet been convincingly demonstrated, because of fundamentally different instrumental requirements. This mode uses secondary electrons or chemical-specific Auger or X-ray-generated emissions that are excited by substantially higher-energy illumination [5]. An energy analyzer is needed to select spectral lines, and to suppress the chromatic aberrations that would otherwise degrade resolution from a wide emission spectrum. Scattering is incoherent, so diffraction and phase contrast plays no role. The angular distribution of emission is diffuse instead of concentrated into bright diffraction spots, hence much larger aperture angles must be used to gather a useful image. Because incoherent scattering does not require parallel, coherent illumination, the incident beam can be highly convergent, and correspondingly more intense. This is fortunate because quantum yields are orders of magnitude lower for Auger lines [5].

With energy filtering, low-voltage secondary emission from several kV illumination should also be interesting. The basic contrast mechanism is similar to SEM, depending upon both yield and local surface inclination. However, since the sample is in a field, the image is also influenced by local lateral gradients near the surface. In general, the spectroscopic mode offers a new set of complementary information from the same basic instrument.

2. Instrument configuration

Fig. 2 is a schematic representation of the SPEC LEEM instrument. The unique elements are shown in more detail, and the path of the field limiting rays is indicated. Conjugate diffraction and image planes are indicated by dots and wavey lines, respectively. The basic elements are the gun/condenser system, the beam separator, the objective lens, the energy analyzing and magnification optics, and the image intensifier/image processor. The beam moves along an inverted Y path, travelling in both directions between the separator and objective. The basic beam energy is 20 keV, but since the sample floats at high voltage, the beam is decelerated and reaccelerated within the objective. The 60° deflection configuration is based on tradition.

A schematic of the high-voltage biasing system is shown. The gun, specimen, objective electrode and energy analyzer supplies are all referenced to a $V_0 = -20$ kV supply that determines the energy of the *imaging* beam. In elastic modes, gun bias V_g is zero, so that the beam arrives at and leaves the sample at specimen start energy V. A field strength $(V_F - V)/z_0$ is applied to the sample at working distance $z_0 = 1$ mm from the focus electrode, so it passes into the magnetic portion of the lens with energy V_F and is further accelerated to energy V_0 before leaving the objective lens.

For secondary imaging modes, the gun voltage is increased to $V_g = 0$ to -3 kV, so that the illuminating beam traverses the optics with an energy $V_0 + V_g$ and is decelerated to a voltage $V_g + V$ before striking the sample. With a sample bias voltage $V = -10$ to $+1000$ V, an illumination energy of -10 to $+4000$ eV is available for mirror mode to Auger excitation. As before, a beam leaving the sample at V is accelerated to V_0 upon leaving the objective. The imaging optics and analyzer are *always* adjusted to accept a 20 keV beam, regardless of illuminating or starting voltage, avoiding the need to readjust the mag-

netic lens, separator and energy analyzer when scanning through the emission spectrum. This biasing scheme is considered essential for convenient operation of the system.

The design of the gun/condenser optics is dictated by the need for a very wide range of current density/coherence at the sample. It has been shown that the LaB_6 flat cathode provides adequate coherence for critical low-angle diffraction, and can deliver much higher currents than other alternatives into the large, convergent-beam probe used for spectroscopy. The elastic imaging modes use a demagnified image of the gun crossover, focused at the objective lens back focal plane. This gives parallel, high-coherence illumination for diffraction and phase contrast. The secondary imaging modes use the illumination optics in a probe-forming mode, focusing an aberrated image of the gun crossover on the specimen with low demagnification. Under correct conditions, this illumination disk can be fairly uniform and very intense. Due to specimen heating and Coulomb interaction effects, the illumination disk should not be much larger than the field of view. A three-condenser-lens system is used to obtain this wide range of illumination conditions. The first two condensers control the crossover demagnification and beam current, while the third condenser and separator jointly focus the crossover near the objective. An illumination aperture is placed midway along the beams path within the separator. This aperture defines the illuminated area of the sample, in the case of secondary imaging by setting the diameter of a caustic disk aberration figure.

The objective lens focuses the image, with 23 × magnification, at the exact center of the separator. For several reasons to be explained later, this condition is vital for both imaging and diffraction. A selected-area aperture for limiting field size is also located here. It also serves to artificially define the center of the separator lens action, minimizing off-axis aberrations. After passing through

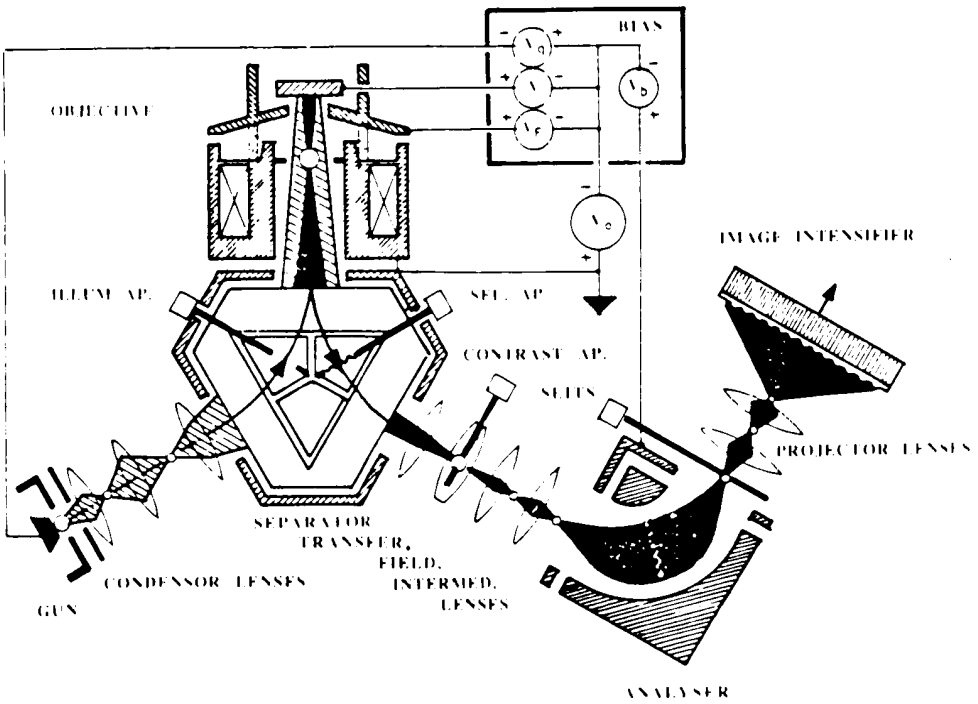

Fig. 2. Schematic of the SPEC LEEM.

the separator, the diffraction plane is refocused by the transfer lens onto the contrast aperture. The transfer lens is the first of four lenses between the separator and energy analyzer, and is there to shorten the system and to precisely refocus the objective back focal plane upon the aperture. This aperture works like a virtual aperture at the objective back focal plane, limiting the angular divergence α at the sample surface. This aperture determines the resolution and collection efficiency of the objective lens. It is removed for viewing the diffraction pattern. The contrast aperture is located at this 0.47 × magnified conjugate plane instead of at the traditional position within the objective lens. If placed within the objective lens, it would also limit the illumination angle in secondary mode, resulting in much lower current density. When apertured as shown, it is also possible to independently align the illumination and imaging paths in the objective lens, resulting in lower off-axis aberrations and simplifying dark-field imaging.

The contrast aperture is exactly at the nodal point of the field lens. This lens forms a real image at the entrance plane of the intermediate lens, which in turn magnifies the image before energy analysis. The field lens focuses the image without influencing contrast aperture conditions. Since the image plane in the separator is fixed, the field lens is used to refocus after changing magnification. In diffraction mode, the intermediate lens focuses on the diffraction plane, essentially reversing the roles of diffraction and image planes in the magnifying optics. By studying the diagram, one can see that the combined action of the separator, objective, transfer and field lens is the surface-imaging equivalent of a TEM objective, and that the rest of the optics is almost identical to an energy-loss TEM.

The balance of the intermediate lens system is designed to meet the optical requirements of the energy analyzer. A 90° decelerating hemispherical analyzer was chosen to be a good compromise between simplicity and resolution/field-of-view requirements. Its optimization will be discussed separately.

The energy window is defined by analyzer slits located at a demagnified diffraction plane. An image appears downstream of this slit. This image is further magnified by the projector lens, appearing finally upon a scintillator screen. This image is transferred light-optically to the intensifier, TV camera and real-time image processor, where it is prepared for viewing on a TV monitor. For recording of more intense images, a 35 mm camera may also directly photograph the screen.

This optics is the synthesis of elastic, inelastic and diffraction imaging requirements. It allows a wide magnification range, and a variety of diffraction modes. Similar to energy-loss TEM configurations, a multi-lens zoom system is needed to prepare the beam for energy analysis. The surface imaging objective optics is inherently more complicated than a TEM objective. In total, the optics is much more complicated than any single mode would require. Nevertheless, a seven-lens configuration has been routinely operated in LEEM II. The key to its successful operation lies in accurate mechanical alignment, minimum lateral magnetic remanences, pre-programed setups, and well developed mutually non-interacting alignment procedures.

3. The objective lens

The objective lens determines performance in imaging modes. In a spectroscopic LEEM, both resolution and collection efficiency are important. The composite electrostatic, electromagnetic triode cathode lens shown in fig. 2 should considerably improve performance in both modes. The properties of this lens have been compared with other alternatives, and published in ref. [8]. The magnetic circuit of the lens uses a double-gap configuration [9] that allows the focus electrode to float at potential $+V_F = 0$ to 7 kV with respect to the sample, but leaves the specimen in an almost magnetic-field-free environment. The floating pole-piece has several advantages. Since the lens aberrations depend primarily upon electric field strength at the sample, the floating pole-piece allows this field to be maximized according to the arc-over tolerances of different samples, which are conservatively estimated to be 30–70 kV/cm. This field can be established using smaller voltages and

gaps while always allowing 20 kV operation of the remaining optics. The alternative of variable working distance is less attractive, because it changes the focal length, which in turn influences all other instrument calibrations. Changes in starting voltage V can also be compensated by V_F to maintain focus, avoiding a change in magnetic excitation. Magnetic changes are accompanied by lateral field variations in the lens bore, which can cause alignment problems in a two-way beam system.

Fig. 3 shows the approximate paths of imaging α-rays and field-limiting γ-rays for elastic and secondary imaging modes. Note the different illumination conditions. Imaging electrons, leaving the surface at angle α and at voltage V, follow parabolic paths in the accelerating field. They enter the magnetic lens at an effective angle $\alpha_0 = \alpha \sqrt{V/V_0}$ from a virtual focus just below the sample. With a net focal length f_0 in high-voltage space, α is defined by a virtual aperture diameter $d_0 = 2\alpha \sqrt{V/V_0}\, f_0$ at the back focal plane. Field rays leaving the edge of a field diameter b_0 cross the back focal plane and emerge at a field angle $\gamma_0 = b_0/2f_0$.

Resolution and aperture angle are determined by the expression:

$$\delta^2 = C_s^2\alpha^6 + C_c^2\alpha^2\,\Delta V^2/V^2 + 0.36K_\lambda^2/\alpha^2 V, \qquad (1)$$

where δ is the resolution, C_s and C_c are spherical and chromatic aberration coefficients, $K_\lambda = \lambda\sqrt{V} = 12 \times 10^{-8}$ cm $\sqrt{V}$ is a diffraction constant, and ΔV is the analyzer energy window. In a well designed cathode lens, aberrations occur predominantly in the very small accelerating region near the sample, so the coefficients are also very small, and the collection angle α can be remarkably large. Bauer has shown that the aberration coefficients of a uniform field F (kV/cm) at the sample are $C_s = C_c \approx V/F$ [10]. These coefficients adequately describe the triode lens properties for this system for the range of $V = 0$ to 500 eV [8].

For high-yield secondary or backscatter imaging, signal statistics are favorable, and high-resolution imaging should be possible. The energy filter may be used to suppress chromatic aberration by choosing the narrowest available window ΔV_{min}. Ref. [6] derives expressions for resolution, aperture diameter and collection factor $\Omega\,\Delta V =$

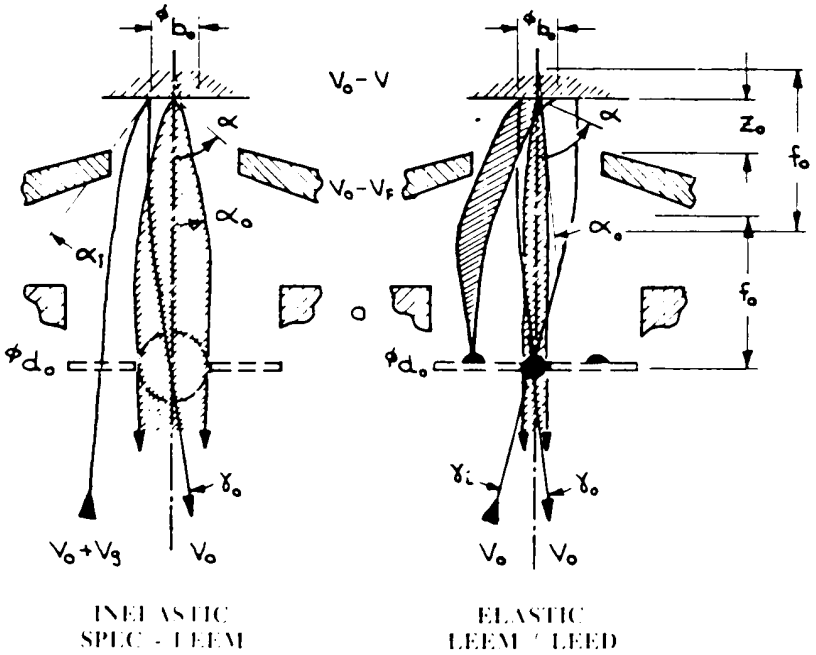

Fig. 3. Operating modes of the objective lens.

$\pi\alpha^2 \Delta V_{min}$ for optimized high-resolution performance as follows:

$$\begin{aligned} d_0 &\approx 1.55 K_\lambda^{1/2} f_0 F^{1/2} V^{1/4} / V_0^{1/2} \Delta V_{min}^{1/2} \\ &\approx 44\ \mu\text{m}, \\ \delta_{min} &\approx 1.55 K_\lambda^{1/2} \Delta V_{min}^{1/2} / V^{1/4} F^{1/2} \\ &\approx 4.6\ \text{nm}, \\ \Omega \Delta V &= 1.88 K_\lambda F / V^{1/2} \\ &\approx 0.004\ \text{sr eV}. \end{aligned} \tag{2}$$

The numbers given are for typical elastic backscatter mode operation of this system, where $F = 7$ kV/mm, $f_0 = 10$ mm, $V = 15$ eV, $V_0 = 20$ keV, and $\Delta V_{min} = 0.2$ eV. The importance of high field strength for both resolution and collection efficiency is clear from these equations. The collection factor is not large when compared to an SEM, where nearly all secondaries in an ~ 5 eV energy window are collected, but it can be shown that when comparable illumination current density is used, the LEEM image statistics would be superior for images containing more than about $5\pi/\Omega \Delta V = 62 \times 62$ pixels.

For spectroscopic imaging, *optimum objective conditions are quite different* because of low scattering yields and high background noise. Resolution will probably be limited by signal statistics and integration times, so the emphasis is upon maximizing the collection factor $\Omega \Delta V$ for *realistic* resolution goals. Expressions for optimum aperture, energy window and collection factor as a function of resolution are given below [6].

$$\begin{aligned} d_0 &\approx 1.57 f_0 F^{1/3} V^{1.6} \delta^{1/3} / V_0^{1/2} \approx 142\ \mu\text{m}, \\ \Delta V_{opt} &\approx 1.08 F^{2.3} V^{1/3} \delta^{2/3} \approx 1.77\ \text{eV}, \\ \Omega \Delta V &\approx 2.13 F^{4/3} \delta^{4/3} / V^{1/3} \approx 0.057\ \text{sr eV}. \end{aligned} \tag{3}$$

The numbers given are for Auger mapping at 30 nm resolution, where $F = 7$ kV/mm, $f_0 = 10$ mm, $V = 100$ eV, and $V_0 = 20$ keV. High field strength is even more important in Auger applications, and start-energy dependences are rather weak. The collection factor is much more favorable than at high resolution, and may be compared with about 0.2π sr eV for a CMA analyzer with 10% transmission viewing a 2 eV wide, cosine-distributed Auger line. Using comparable current density, the SPEC LEEM should be superior for images containing more than 3×3 pixels. In the SPEC LEEM, the key to good inelastic imaging will be the correct choice of illumination, aperture and energy window conditions based on *pre-calculated* realistic resolution goals. Fig. 4 shows optimum conditions over the full range of anticipated resolutions for $V = 100$ eV, $V_0 = 20$ keV, $f_0 = 10$ mm, $F = 7$ kV/mm.

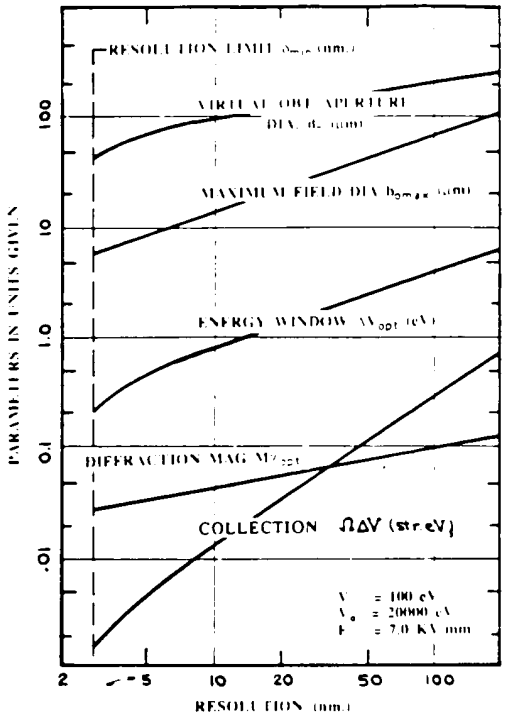

Fig. 4. Parameters for optimum collection efficiency and field of view as function of resolution chosen to give a visible image.

4. The separator

The magnetic separator is a passive optical element whose function is to transfer images and diffraction patterns with a minimum of astigmatism, distortion and aberration. Prisms act as long-focal-length lenses, whose properties are typically asymmetric in the horizontal and vertical focusing planes. They are also subject to large second-order aberrations of dipole fields. In a

spectroscopic LEEM, the separator must accommodate the adjustable energy difference V_g of several keV between the illuminating and imaging beam, without shifting any of the three optical axes.

These requirements forced the development of a 60° deflecting "close-packed prism array" whose concept is new to electron microscopy [11]. The concept is extended to 90° deflection and its ray optics are treated in detail in a publication submitted to OPTIK [12]. In brief, the prism array, whose active pole-pieces are shown in fig. 2, consists of an outer-shell shield and flux shunt, surrounding a triangular ring pole-piece, which in turn surrounds three differentially excited inner pole pieces. It is mechanically symmetric about the three beam axes, and is both mechanically and magnetically symmetric about the bisectors of these axes. This insures that centers of deflection coincide with the mechanical center of the array. The inner prism segments act independently upon the illuminating and imaging beams, so that differential excitations compensate for energy differences with minimum mutual interaction.

The first-order focusing properties in the horizontal and vertical planes depend upon both the geometry and the relative excitations of the inner and outer pole-pieces, which determine deflection angles $2\Phi_1 + \Phi_2 = 60°$ in the different prism elements. Vertical focusing occurs only at the inner edge transitions, and is convergent when the outer excitation is larger than the inner. Horizontal focusing is convergent within the sectors but is divergent at the inner edge transitions [13], so it is possible to equalize the net focusing action in both planes. There exists an optimum combination of inner and outer excitations, where the system behaves almost like a thin, axially symmetric lens for all image and object positions. Specifically, both the diffraction and image planes may be transferred without first-order astigmatism or distortion. The important parameters for this system are $\Phi_1 = 21.8°$, $R_1 \approx 70$ mm, and $\Phi_2 = 16.4°$, $R_2 \approx 145$ mm. Under these conditions, focal lengths $f_H = f_V \approx 170$ mm. These properties have been verified in LEEM II and later modeled by M. Mankos in unpublished work. The key to the correct function of this element is high permeability, low-remanence magnetic materials, and the use of absolutely non-magnetic vacuum system materials.

There are several characteristics of the separator/objective lens system that are important but not immediately obvious. Image resolution is determined mostly by the objective lens, but also by aberrations along the image side path through the separator. For elastic imaging and diffraction, parallel illumination is important, and is insured by minimum astigmatism and aberration along the illumination path. For diffraction, the sample acts like a multifaceted mirror, so that astigmatism and aberration along the illumination path are reflected into each diffraction spot, and combine with image path astigmatism and aberration to determine the combined transfer characteristics for diffraction.

The specimen image is focused by the objective lens onto a plane midway through the image side of the separator. This plane is a principal plane for the lens action of the separator, so its influence upon image focusing is minimum. This plane is also an achromatic plane, so that if focused here, the image is free of dispersion (transverse chromatic aberration).

The same objective focus applies for good diffraction performance, because it minimizes the diameter of the beam within the separator. A favorable diffraction transfer width (small spots) requires high coherence (small crossover at the exit of the condensor lenses), and also requires that this crossover image be transferred through both illumination and image side paths with minimum dispersion, astigmatism and aberration. Castaing has pointed out that this transfer is achromatic because the objective acts as an inverting mirror [14]. The path of the central ray emerging from the entire separator/objective system is not influenced by small source energy spread or by high voltage or separator field instabilities. This characteristic is exploited not only to improve diffraction performance, but also to find the beam despite its complicated path. We use this achromatic property to focus the objective while wobbling the inner magnetic prism excitations.

Symmetries are also exploited to minimize low-order dipole aberrations in the separator [15].

When the objective is properly focused, imaging rays from a point at the center of the specimen pass antisymmetrically through the image side separator, cancelling second-order axial dipole image aberrations. Similarly, field rays originating from the condensor crossover pass antisymmetrically through the illumination and image sides of the separator; those following an inner path on one side are reflected by the specimen/objective in such a way that they follow outer paths on the other side. Thus the entire transfer of diffraction spots is free of second-order axial aberrations even though the spots are aberrated at the objective back focal planes. Off-axis field aberrations are reduced but not eliminated by objective focus. All these imaging characteristics derive automatically from the inherently astigmatism-free pole-piece arrangement and from attention to objective focus. They are harder to realize using external quadrupole correctors that tend to behave as "thick" lenses with residual distortion and alignment problems. We believe that the prism array separator improves performance and simplifies the optics by minimizing the problems associated with the use of large-angle bending magnets in an otherwise axially symmetric beam path.

The dispersion of the separator is about 5 μm/eV, reflected onto the objective back focal plane. Comparing this to the 40–200 μm apertures used here, it is clear that the separator is not useful for high-resolution energy analysis. However, with the aperture placed after the separator, the dispersion is used advantageously to pre-filter the image. Provided the Auger peaks in the spectrum are far enough away from much stronger secondary and backscatter peaks, most of the background emission may be removed at the contrast aperture. This should make conditions in the analyzer more favorable. For similar reasons, one may expect unfiltered elastic backscatter images to be free of the defocused secondary image that otherwise reduces contrast and emphasizes uninteresting topography.

5. The spectroscopic imaging system

The imaging system magnifies and energy-analyzes the image. Its design is dictated by the necessary magnification range, diffraction requirements, and in particular by the properties of the analyzer itself. We first consider a "black box" model of the imaging system as a whole, from which the important relationships are derived.

A generalized imaging system is shown in fig. 5. The objective lens input is shown on the left. The aperture diameter $d_0 = 2\alpha f_0 \sqrt{V/V_0}$ and the field angle $\gamma_0 = b_0/2f_0$ are fixed for an optimized setup $\delta(\alpha_{opt}, \Delta V_{opt})$, and for a field of view of n pixels, where $b_0 = n\delta$. The task of the black box is to magnify the image to diameter b_4, to demagnify the aperture to diameter d_4 at a location a dis-

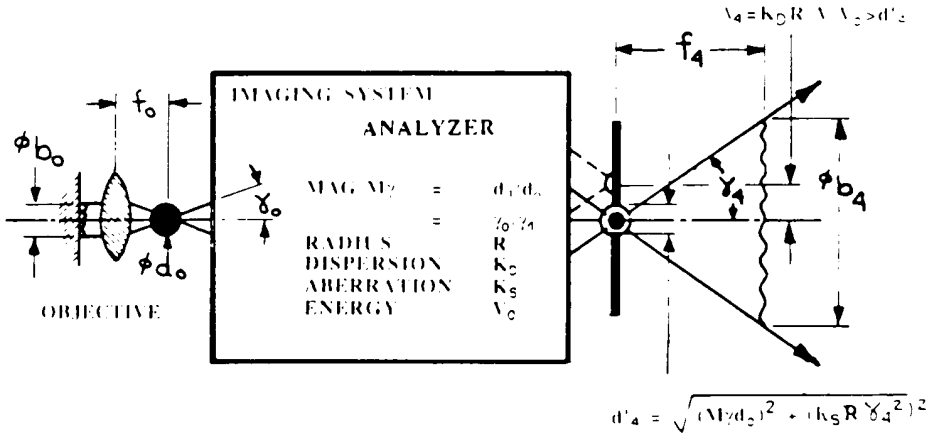

Fig. 5. Black box model of analyzer and magnifying optics.

tance f_4 in front of the image, and at this point to energy-analyze the image with a window ΔV. The image magnification is $M_a = b_4/b_0$, and the diffraction plane magnification is $M_\gamma = d_4/d_0$. By conservation of phase space, $d_0\gamma_0 = d_0 b_0/2f_0 = d_4\gamma_4 = d_4 b_4/2f_4$, so that the magnifications are related by the formula:

$$M_a = f_4/f_0 M_\gamma. \tag{4}$$

The analyzer section of the black box has an energy dispersion and aberrations whose coefficients may be expressed in output space no matter where it is within the system. The effect of dispersion is to displace aperture image d_4 by a distance $K_D R\,\Delta V/V_0$. The effect of a dominant second-order aberration in the analyzer is to increase diameter d_4 by an amount $K_S R\gamma_4^2$, where K_D and K_S are dispersion and aberration coefficients, and R is a characteristic length or radius of curvature in the analyzer.

To energy-analyze the image, a slit is placed at plane d_4, so that only electrons in energy band ΔV pass on to the final image. This slit cannot be smaller than aperture image d_4, for otherwise it would artificially limit the aperture angle α. The image d_4 must also be accurately focused at the slit, so that field b_0 is not artificially limited. The condition for energy analysis is $d_4 = Md_0 \le K_D R\,\Delta V/V_0$. The aperture image must be demagnified until this condition is met. When the aberration associated with a finite field size is included, the condition for energy analysis of entire field becomes

$$K_D^2 R^2\,\Delta V^2/V_0^2 \ge M_\gamma^2 d_0^2 + K_S^2 R^2 \gamma_4^4 \ge M_\gamma^2 d_0^2 + K_S^2 R^2 b_0^2/16 f_0^4 M_\gamma^4, \tag{5}$$

where $\gamma_0 = b_0/2f_0$ has been substituted for $\gamma_4 = \gamma_0/M_\gamma$.

Thus there is an optimum choice of M_γ that will allow a maximum field of view at the required energy window. Solving eq. (5) for b_0 and maximizing with respect to M_γ,

$$M_{\gamma\,\mathrm{opt}} = \left[\frac{0.81 K_D R}{V_a}\right]\frac{\Delta V}{d_0},$$
$$b_{0\,\max} \le \left[\frac{1.24 f_0 K_D^{3/2}}{K_S^{1/2} V_0^{3/2}}\right]\frac{\Delta V^{3/2}}{d_0}. \tag{6}$$

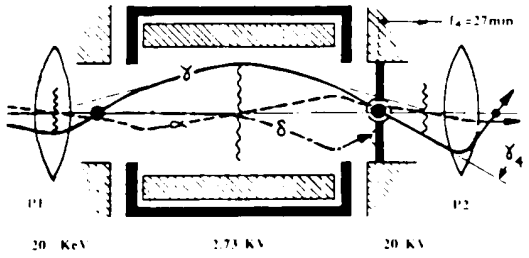

Fig. 6. Energy-analyzer optics.

The general equations (4) and (6) specify the properties of the intermediate lens system, that must be placed before an analyzer to insure matching for maximum field of view and energy window.

Section 3 gives the values of d_0 and ΔV in the objective lens in terms of resolution. These may be inserted into eq. (6) to obtain M and pixel count $n = b_{0,\max}/\delta$ that can be obtained with a given analyzer:

$$M < \left[\frac{0.55 K_D R}{V_0^{1/2} f_0}\right] F^{1/3} V^{1/6} \delta^{1/3},$$
$$n < \left[\frac{0.81 K_D^{3/2} R}{K_S^{1/2} V_0}\right]\left[\frac{V^{1/3} F^{2/3}}{\delta^{1/3}}\right]. \tag{7}$$

Since pixel count and objective optimization cannot be compromised, the last equation places non-negotiable requirements upon the properties of the analyzer.

For the SPEC LEEM, we have chosen a hemispherical plate analyzer that acts upon a decelerated beam. Fig. 6 shows the approximate ray paths through the analyzer, as though the curved axis were a straight line. The hemispherical plates are within an enclosure with round entrance and exit holes. The assembly floats at $V_b = +2738$ V with respect to the 20 keV reference supply, so the beam passes through with energy V_b and radius of curvature $R = 50$ mm. In low-voltage space, the dispersion is 35 μm/eV and the aberration coefficient is $7.36R$.

The decelerating and accelerating lenses at the ends of the analyzer transfer the image plane in P1 to the achromatic plane at the center of the analyzer, and then to the plane outside the analyzer. The diffraction plane is transferred to energy slit plane outside the analyzer at ground

potential. Angle γ_4 is reduced within the hemispheres. Meslik and Chmelik [16] have computed the properties of the entire analyzer system, using both analytical and ray-tracing techniques. Its properties may be expressed in high-voltage V_0 space for the transfer of diffraction and image planes as follows:

$$
\begin{aligned}
&M_{\gamma A} = d_6/d_4 = 1.13\times,\\
&M_{\alpha A} = b_6/b_4 = 1.0\times,\\
&K_D = 2.67\ (6.8\ \mu\mathrm{m/eV}),\\
&K_S = 0.224,\\
&f_4 = 27\ \mathrm{mm}.
\end{aligned}
\tag{8}
$$

The dispersion of the system is not particularly large in high-voltage space, but as a consequence of deceleration, the important ratio $K_D^{3/2}/K_S^{1/2}$ in eq. (7) is much more favorable than can be obtained using simple magnetic sectors.

Using this data, the optimum intermediate magnifications M_γ or M_α, the field limitations and pixel counts for the imaging system are:

$$
\begin{aligned}
&M_\gamma = 2.1/M_\alpha \le 0.051\left[F^{1/3}V^{1/6}\delta^{1/3}\right]\\
&\quad \approx 0.023\text{–}0.10,\\
&b_{0,\max} \le 0.0019\left[V^{1/3}F^{2/3}\delta^{2/3}\right]\\
&\quad \approx 3.9\text{–}69\ \mu\mathrm{m},\\
&n \le 0.0019\left[V^{1/3}F^{2/3}/\delta^{1/3}\right]\\
&\quad \approx 1114\text{–}686\ \mathrm{pixels}.
\end{aligned}
\tag{9}
$$

The two numerical estimates are for $F = 7$ kV/mm, and resolution $\delta = 4.6$ nm at 15 eV, and $\delta = 100$ nm at 100 eV respectively.

The intermediate demagnification M_γ and image spacing f_4 associated with the analyzer dictate the detailed design of the intermediate lens optics. Separator properties and certain diffraction requirements also play a role. Fig. 7 shows lens configurations and typical ray traces for typical high-magnification and diffraction modes in the intermediate lens system. The functions of most of the lenses have been described in section 2. Projector lens 1, just before the analyzer, is placed at image plane b_4 so that it can be used to focus the analyzer without influencing image focus and magnification. Diffraction mode has the net

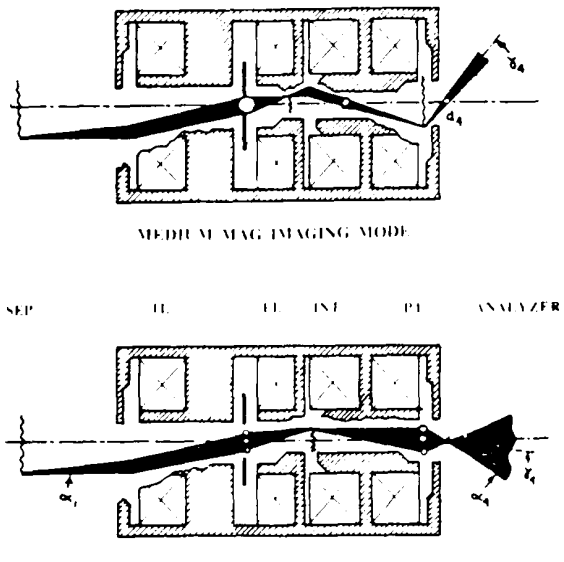

Fig. 7. The intermediate optics in imaging and diffraction modes.

effect of reversing planes b and d in fig. 6, so that diffraction patterns may also be energy-filtered.

Lens spacings and minimum focal lengths are chosen to provide a range $M_\gamma = 0.015$–0.1, or an image magnification of $M_\alpha = 140$–$21\times$. Intermediate lens excitation is chosen according to resolution, and then PI and field lens are set to focus the analyzer and image respectively. Using this procedure, one may be reasonably certain that correct values of M_γ are used in practice. Chmelik has computed nominal setup conditions in terms of lens currents versus M_γ for all modes, using vector potential programs, giving a starting point for tuning the instrument [17].

The design range for field of view (i.e., total magnification) is 0.5–50 μm. Using the full range of intermediate lens magnification, the image at the end of the analyzer is 10 to 1000 μm diameter. A double-gap projector lens with a useful magnification range of 10–$120\times$ is used to project the final image on the 10 mm diameter screen. The depth of field of the magnified image is sufficient to make it seem to behave like a zoom lens.

6. The image detector

In the elastic imaging LEEM II instrument, images are sometimes intense enough to be observed on a phosphor screen. Spectroscopic images will be many orders of magnitude weaker, and will have very low contrast. Under this range of conditions, an image intensifier with a wide sensitivity range and favorable quantum-noise-limited statistics is needed. In addition, selective contrast enhancement will be needed before an image may be viewed or recorded.

We propose to extract weak Auger images from the background using a technique familiar to scanning Auger microscopy. The analyzer deflectors can be toggled between two pass energies synchronous with subharmonics of the TV frame rate, so that images at the two energies can first be integrated, stored, and then subtracted using an on-line image processor. Exposed in this way, the image is the difference between images taken at, and adjacent to, the Auger peak, which enhances contrast but does not eliminate background noise. The toggling frequency is low enough to integrate many frames, but high enough to allow real-time focusing and specimen movement. The subtracted image is digitally recorded, and the viewing monitor display is updated at the end of each toggle cycle. When image statistics require longer integration times, the pre-averaged data can be again routed through the image processor for further averaging and subsequent display, or can be post-processed off-line.

The image intensifier design faces two major problems: high quantum efficiency and wide operating range. Maximum current densities in the final image occur in mirror and LEED modes, where several tens of μA beam current can fall upon the scintillator screen. Lowest current densities are encountered in Auger imaging, where a signal-to-noise ratio of 1 in a 50×50 pixel image integrated for 100 s implies a beam current of 10^{-17} A. The detector must be both robust and sensitive.

The detection quantum efficiency is the square of the actual to quantum-limited signal-to-noise ratio in each pixel. It may also be thought of as the attenuation of the useful signal due to imperfect detection, so the integration time necessary to record a quantum-noise-limited image increases with 1/DQE . The essential condition for the DQE to approach unity is that each of the first few stages of the multipication chain have a sufficiently high quantum gain, in other words that the flux increase after each multiplication. It is also important that the net multiplication be larger than one under intense diffraction and backscatter and weak spectroscopic imaging conditions. A treatment of the statistics of image intensifiers may be found in ref. [18].

The DQE of a channel plate placed directly in the 20 keV beam is poor because the secondary coefficient of the input surface is low for high-energy electrons. In addition, experience has shown that detector flux densities that can permanently damage the detector are difficult to avoid. It would be desirable to provide variable attenuation before the intensifier.

A light-optical-coupled intensifier seems to offer a better (but untried) solution to both problems. A YAG scintillator crystal combines high resolution, insensitivity to damage, and adequate photon yield. Using a conventional F 1.2 macro-lens with 20 mm focal length and $4 \times$ magnification, about 10% of the light yield of a 10 mm screen may be collected and projected upon a 40 mm photocathode/microchannel plate system. The lens may be automatically apertured to attenuate bright images and protect the intensifier. This aperture increases the operating range by about $1000 \times$ without requiring that the MCP be operated under unfavorably low gain conditions. The channel plate output is on a second phosphor or YAG screen viewed by a conventional low-light camera. The dynamic range may be covered by aperturing both lenses and controlling the channel plate gain. With a scintillator yield of $150 \times$, a 10% lens transmission, a 20% photocathode yield, and a $5 \times$ interstage multiplication in the MCP, the predicted DQE is 0.5–0.7. While not perfect, it seems that this detector would be acceptable.

7. Specimen systems

The SPEC LEEM is intended for the dynamic observation of surface phenomena. Ultrahigh

vacuum and associated sputtering, heating, evaporation and gas-handling systems are needed. The specimen chamber and optics are fully metal-sealed construction. Nominal pressure is 6×10^{-11} Torr, reached after a 10 h bakeout at 170°C. Specimens are introduced through a two-stage airlock. The first stage is turbo-pumped to about 10^{-7} Torr, after which the specimen is transferred to an ion-pumped preparation chamber. Here the specimen and cartridge are outgassed by an auxiliary bombardment heater, and the surface is sputtered if required. It is then transferred to the observation position. A transfer from atmospheric pressure to 2×10^{-10} Torr takes about 1.5 h. After sufficient in-situ outgassing, suitable samples may be observed at 1000°C at 3×10^{-10} Torr.

The sample is mounted on a cartridge that also carries the specimen bombardment heater and thermocouple-monitored ballast ring contacting the back side of the sample. This ring allows sample exchange without reconstruction of the thermocouple junction. The bombardment heater irradiates both the ring and the back of the sample. With proper choice of ring geometry, the heater flux and thermal losses in the ring and sample may be balanced so that their thermal behavior is correlated in spite of imperfect contact. With 75 W bombardment power, the sample may be flashed to 1600°C. The thermal time constant and stability are about 4 s and ± 0.25°C, allowing quantitative observation of phase transitions under controlled cooling rates.

The specimen is visible through eight 14° conical holes at 16° incidence. These holes are used for evaporation, gas exposure, ion bombardment, pyrometer observation, and for the Hg UV lamp for PEEM. These sources are baffled and apertured to avoid contaminating optical elements.

8. Experimental techniques

The design of a new instrument requires a clear, although preliminary, picture of how it is to be used. This assures that necessary elements are not forgotten, and leaves the experimentalist with some idea of the designer's intent. This shortens, but does not avoid, the period of trial and error before the instrument becomes productive. In this spirit, a typical experimental sequence is offered as a review of the important points in the previous sections.

Spectroscopic imaging of unfamiliar samples will be difficult because of low contrasts and yields, which in turn imply long integration times. Not only optimum instrumental conditions but also considerable foreknowledge of the sample may be necessary before an image becomes visible. In particular, where chemical contrast comes from small localized regions, it becomes necessary to tune the instrument for high resolution without having a visible chemical contrast image. The instrument is designed to support procedures for quick adjustment and sample characterization/survey leading up to spectroscopic imaging.

Except for flatness and conductivity, mirror imaging makes no demands upon the sample's topography, structure and composition. It is well suited for preliminary adjustment of alignment and illumination conditions. Using a slightly convergent illumination beam, a dark spot within the illuminated field represents the transition between mirror and absorption conditions. A round, centered spot that breathes with condensor, objective, and imaging lens focus indicates correct stigmation and alignment of the illumination beam. A large uniform field for mirror imaging indicates the parallel illumination conditions necessary for elastic LEEM/LEED imaging. Correct objective and field lens focus can be established by wobbling various prism excitations.

Larger topographic detail is visible in mirror mode. On monocrystalline samples, LEED and elastic backscatter LEEM/LEED modes are useful for determining the cleanliness and step structure before beginning to study epitaxial growth or localized chemistry. PEEM is useful for limited topographic and chemical characterization, especially on polycrystalline or amorphous samples that preclude elastic contrast. These modes are also useful for monitoring in-situ thermal, evaporation and sputtering treatments with favorable image statistics.

The transition from elastic to secondary/Auger contrast modes is likely to be difficult because of

low yield and elemental contrast, and because of the changes in illumination energy and intensity necessary to obtain favorable image statistics. A high-resolution, low-noise way of viewing the specimen during the transition is highly desirable for instrumental setup and for finding interesting areas on the sample. The high-voltage biasing and the separator prism systems are designed to allow minimum readjustment of the imaging beam path while readjusting the illumination for secondary/Auger imaging. The illumination energy bias V_g and the inner prism of the illumination beam may be adjusted to keep the illumination field centered. The gun emmission and condensor lens magnification/aperture may be adjusted to exactly fill the field of view with the most intense illumination allowed by specimen damage and Coulomb interaction effects.

During the setup procedure, low-voltage secondary electron images will be useful because of their high quantum yield and reasonably narrow energy spread. If specimen areas with favorable topography can be found, optimum apertures and energy-analyzer slits can be introduced, and alignment, stigmation and focus can be adjusted using intense, high contrast images. With energy analysis, these secondary images should have quite good resolution.

It is particularly important that final spectroscopic imaging conditions be set up with a specific resolution and field of view in mind, because optimum collection efficiency, illumination setup, intermediate lens magnification and energy window all depend upon the resolution. To choose a realistic resolution goal, a foreknowledge of specimen quantum yield and contrast is desirable. The yield and pixel size δ determine the signal-to-noise ratio with each pixel, and the spatial contrast between pixels determines the signal-to-noise threshold and integration time necessary to make the Auger image contrast visible.

The instrument allows the quantum yield and Auger line spectral contrast to be determined from an unresolved image. This is done by varying the specimen voltage V while summing all pixels in the image. With foreknowledge of yields, and spectral line energies the system may be retuned using the much brighter secondary images.

For favorable samples, dynamic imaging of Auger electrons may be possible, but for high-resolution imaging of weak samples, the final transition to Auger imaging may have to be done blind – that is, without focusing or moving the sample. Sample voltage and focus voltage V_F can be set to pre-calibrated values, and the real time integration and background subtraction program in the image processor can be activated. After the necessary integration interval, the Auger image becomes visible. The mirror LEEM/LEED, PEEM and secondary images obtained during setup serve as complementary data sets showing different characteristics of the sample. When dynamic processes such as thermal cycling, evaporation or sputtering are reversible, then complementary data sets using different imaging modes may be exposed under reproducible conditions.

This imaginary sequence summarizes our hope that the instrument will contribute interesting new results.

Acknowledgements

The author acknowledges the support of the Volkswagen Foundation, the inspiration and leadership of Professor E. Bauer, and the very substantial contributions of W. Święch, M. Mundschau, G. Marx, H. Pinkvos, J. Chmelik, M. Mankôs, J. Meslik, V. Kolarik, M. Lenć, B. Lencóva, C. Eisefelder and many others, both directly to this work and to the education of the author.

References

[1] R.A. Schwarzer, Microsc. Acta 84 (1981) 51.
[2] V. Drahos, A. Delong, V. Kolarik and M. Lenć, J. Microscopie 18 (1973) 133.
[3] E. Bauer, in: Proc. 5th Int. Congr. on Electron Microscopy, Philadelphia, 1962, Vol. D II, Ed. S.S. Breese (Academic Press, New York, 1962).
[4] E. Bauer, M. Mundschau, W. Święch and W. Telieps, Ultramicrosocpy 31 (1989) 49.
[5] E. Bauer and W. Telieps, Emission and low-energy reflection microscopy, in: Study of Surface and Interface Characterization by Electron Optical Techniques, Eds. A. Howie and U. Valdrè (Plenum, New York, 1988).

[6] L. Veneklasen, Ultramicroscopy 36 (1991) 63.
[7] E. Bauer, L. Veneklasen, W. Święch, G. Marx and H. Pinkvos, unpublished.
[8] J. Chmelík, L. Veneklasen and G. Marx, Optik 83 (1989) 155.
[9] J. Chmelík, Optik 81 (1989) 103.
[10] E. Bauer, Ultramicrosocpy 17 (1985) 51.
[11] L. Veneklasen and G. Marx, unpublished.
[12] M. Mankôs, V. Kolarik and L. Veneklasen, Optik, submitted.
[13] H. Enge, in: Focusing of Charged Particles, Ed. A. Septier (Academic Press, New York, 1967) p. 203.
[14] R. Castaing, in: Focusing of Charged Particles, Ed. A. Septier (Academic Press, New York, 1967) p. 291.
[15] H. Rose, Optik 51 (1978) 15.
[16] J. Chmelík and J. Meslik, unpublished.
[17] J. Chmelík, private communication.
[18] K.-H. Herrmann and D. Krahl, in: Advances in Optical and Electron Microscopy, Vol. 9, Eds. R. Barer and V.E. Cosslett (Academic Press, New York, 1984).